Solar Phys (2009) 260: 177–189
DOI 10.1007/s11207-009-9421-y

Relative Kinematics of the Leading Edge and the Prominence in Coronal Mass Ejections

Darije Maričić · Bojan Vršnak · Dragan Roša

Received: 12 March 2009 / Accepted: 24 July 2009 / Published online: 14 August 2009

Abstract We present a statistical analysis of the relationship between the kinematics of the leading edge and the eruptive prominence in coronal mass ejections (CMEs). We study the acceleration phase of 18 CMEs in which kinematics was measured from the pre-eruption stage up to the post-acceleration phase. In all CMEs, the three part structure (the leading edge, the cavity, and the prominence) was clearly recognizable from early stages of the eruption. The data show a distinct correlation between the duration of the leading edge (LE) acceleration and eruptive prominence (EP) acceleration. In the majority of events (78%) the acceleration phase onset of the LE is very closely synchronized (within ± 20 min) with the acceleration of EP. However, in two events the LE acceleration started significantly earlier than the EP acceleration (> 50 min), and in two events the EP acceleration started earlier than the LE acceleration (> 40 min). The average peak acceleration of LEs (281 $\mathrm{m\,s^{-2}}$) is about two times larger than the average peak acceleration of EPs (136 $\mathrm{m\,s^{-2}}$). For the first time, our results quantitatively demonstrate the level of synchronization of the acceleration phase of LE and EP in a rather large sample of events, *i.e.*, we quantify how often the eruption develops in a "self-similar" manner.

Keywords Sun: coronal mass ejections (CMEs) · Sun: prominences

1. Introduction

Coronal mass ejection (CME) is a large-scale eruptive solar phenomenon, launching 10^{11} – 10^{13} kg of coronal plasma into interplanetary space at speeds ranging from several tens of $\mathrm{km\,s^{-1}}$, up to more than 2000 $\mathrm{km\,s^{-1}}$ (*e.g.*, Gopalswamy (2006) and references therein). Observations show that kinematic evolution of CMEs can be divided into three distinct

D. Maričić · D. Roša
Zagreb Observatory, Zagreb, Croatia

B. Vršnak (✉)
Hvar Observatory, Faculty of Geodesy, University of Zagreb, Zagreb, Croatia
e-mail: bvrsnak@geof.hr

phases: *i*) a slow rising motion (this phase may last for hours, and is usually considered to be a quasi-stationary evolution of the pre-eruptive structure through a series of equilibrium states); *ii*) main acceleration phase lasting from several minutes up to several hours; *iii*) post-acceleration phase, showing approximately a constant velocity or a weak residual acceleration/deceleration (*e.g.*, Maričić *et al.* (2004) and references therein). The first two phases generally occur in the inner corona, while the third phase takes place at larger coronal heights.

The CME take-off can be very impulsive – in extreme cases the acceleration is so strong that CME achieves a velocity on the order of 1000 km s^{-1} in less than 10 min (*e.g.*, Vršnak, 2001; Zhang *et al.*, 2001; Gallagher, Lawrence, and Dennis, 2003; Williams *et al.*, 2005; see also Vršnak *et al.* (2007) and references therein). On the other hand, there are very gradual events whose acceleration lasts for several hours, never exceeding 100 m s^{-2} (*e.g.*, Zhang *et al.*, 2004). The fastest CMEs are usually related to an impulsive acceleration, but not necessarily, since occasionally fast events show a gradual acceleration (Vršnak, Sudar, and Ruždjak, 2005). Apparently, the kinematic properties are related to the characteristics of the environment: impulsive events are usually launched from active regions and are tightly related to solar flares, whereas the events launched from quiet regions are usually more gradual (Andrews and Howard, 2001; Maričić *et al.*, 2007). Furthermore, the impulsiveness of the acceleration depends on the source-region size; initially large structures are accelerated more gradually than compact structures (Vršnak *et al.*, 2007).

Early CME studies revealed that the most frequent low-coronal activity associated with CMEs are eruptive prominences (Munro *et al.*, 1979; Webb, Krieger, and Rust, 1976; Webb and Hundhausen, 1987). On the other hand, it was found that CMEs often expose a three-part structure (*cf.*, Hundhausen, 1987): the leading edge (LE), the cavity, and the bright core. Subsequently, various case studies (*e.g.*, House *et al.*, 1981; Illing and Hundhausen, 1985) clearly demonstrated that the bright core of the white-light CME corresponds to the eruptive prominence (EP). In this respect, it should be noted that observations in EUV, soft X-rays, and the solar-eclipse observations revealed that the pre-eruptive prominence/corona structures show a similar pattern: prominences are usually found in a coronal void nested in the arch of the helmet streamer (*cf.*, Engvold, 1987; see also Maričić *et al.* (2004) and references therein), indicating that the basic CME morphology has its roots in the pre-eruption magnetic field configuration.

Generally, EPs are considered to be just a consequence of the CME phenomenon (*cf.*, Hundhausen, 1999). However, there are alternative viewpoints that pay more attention to the core of the erupting structure, *i.e.*, those parts imbedding the prominence plasma (*e.g.*, Vršnak, Ruždjak, and Rompolt, 1991; Filippov, 1998; Filippov and Koutchmy, 2008; Koutchmy *et al.*, 2008). Thus, detailed studies of the height, speed, and acceleration time-profiles of different CME structural components are essential for comprehension of the initiation process and the dynamics of CME until late phases of eruption. A number of studies presented indications of synchronized kinematics of different parts of the CME (Schmahl and Hildner, 1977; Fisher, Garcia, and Seagraves, 1981; Illing and Hundhausen, 1985; Low and Hundhausen, 1987; Plunkett *et al.*, 1997; Dere *et al.*, 1999; Wood *et al.*, 1999; Srivastava *et al.*, 2000; Plunkett *et al.*, 2000; Krall *et al.*, 2001; Maričić *et al.*, 2004; Koutchmy *et al.*, 2008). However, in most of these studies, the "self-similarity" of the CME expansion is well-documented only for late phases of the eruption, when the eruption already entered into the constant-velocity regime (*e.g.*, Wood *et al.*, 1999; Koutchmy *et al.*, 2008). The situation is much less clear for the acceleration phase itself. For example, Schmahl and Hildner (1977), Illing and Hundhausen (1985), and Koutchmy *et al.* (2008) traced the acceleration of the eruptive prominence, but their observations did not capture the acceleration

phase of the CME leading edge. Consequently there is no information about the synchronization of the LE and EP acceleration. Fisher, Garcia, and Seagraves (1981), Low and Hundhausen (1987), Plunkett *et al.* (1997), and Krall *et al.* (2001) traced the acceleration of both CME components, but no definite conclusion can be drawn due to a too large noise in the data and/or a too low resolution; Dere *et al.* (1999) presented the EP/LE relationship only qualitatively, and so on.

Furthermore, in most of the previously mentioned studies, only the height – time data are presented, covering a large time – distance range. In such a presentation, dominated by the post-acceleration stage, the acceleration phase covers only a small fragment of the presented data, so it is not possible to clearly resolve the relative timing of the EP and LE accelerations. Yet, the measurements shown by Fisher, Garcia, and Seagraves (1981) and Plunkett *et al.* (1997, 2000) might indicate that the LE starts to accelerate before the EP.

The only studies directly comparing the acceleration – time profiles of both LE and EP were presented by Srivastava *et al.* (2000) and Maričić *et al.* (2004). The measurements by Maričić *et al.* (2004) revealed a very high level of self-similarity of the eruption, including synchronization of the acceleration stage with the impulsive phase of the associated flare. On the other hand, Srivastava *et al.* (2000) analyzed in detail a gradual CME (acceleration phase lasting for several hours) and found that the EP acceleration was delayed with respect to the LE acceleration for about 2 h. Combining this with the actual magnetic field properties of the erupting structure, Srivastava *et al.* (2000) concluded that the prominence lost equilibrium as a consequence of the eruption of the overlaying magnetic field structure. It is interesting to note that, in this event, the LE and EP acceleration started at different times, but at approximately equal height. The presented state of the art reveals that the self-similar CME expansion is well documented for the post-acceleration stage of the eruption, but that the situation during the CME initiation phase is far from being conclusive. Thus, further detailed quantitative studies of the acceleration phase are necessary.

In this article, we focus specifically on the self-similarity of the eruption during the acceleration phase. Given this goal, we analyzed the acceleration – time profiles for a relatively large sample of well-observed events, following the procedure described by Maričić *et al.* (2004). All selected events were recorded by the same set of three instruments: the Extreme Ultraviolet Telescope (EIT; Delaboudiniere *et al.*, 1995) onboard the Solar and Heliospheric Observatory (SoHO), Mark-IV K-coronameter (MK-IV) of the Mauna Loa Solar Observatory (MLSO), and Large Angle and Spectrometric Coronagraph (LASCO; Brueckner *et al.*, 1995) onboard SoHO, which makes the comparison between event characteristics more reliable. In Section 2 we present observations, the event selection, and the method to determine characteristics of the main acceleration phase of LEs and EPs. The results of statistical analysis are given in Section 3. Conclusions are drawn in Section 4.

2. Observations and Measurements

Our sample consists of 18 events with a clearly recognizable three-part structure. The only selection criterion was that the kinematics of EP and LE could be measured reliably from the gradual pre-acceleration phase, up to the post-acceleration stage. Most of the events occurred close to the solar limb. The kinematics of the eruption was measured employing the data recorded by EIT/SoHO, MK-IV/MLSO, and LASCO/SoHO. The EIT Fe XII 195 Å data were used to trace the EUV coronal structures in the early stages of the eruption. The EIT has a field-of-view of 1.4 solar radii and Fe XII 195 Å images reveal coronal structures at temperatures around 1.6 MK. The MK-IV instrument has a field-of-view from 1.1 to 2.8 solar radii. At larger heights, CMEs were traced employing the C2 and C3 white-light images

of LASCO, which cover radial distance ranges 2.2 – 6 and 4 – 30 solar radii, respectively. The combined EIT, MK-IV, and LASCO data enable a complete analysis of the CME kinematics, including the initiation, the acceleration phase, and the propagation phase. In this respect, the MK-IV coronagraph provides the key measurements of the CME acceleration in the majority of analyzed events.

The CME kinematics was measured by tracing the tip of LE and the tip of EP. The analysis of kinematics is based on the smoothed height – time measurements of LE and EP (for details see Maričić *et al.* (2004)), providing the velocity and acceleration time-profiles. From these profiles we estimated the onset and the end of the acceleration phase (t_b and t_e, respectively), the duration of the acceleration phase ($T_a = t_e - t_b$), the peak velocity, v_m, the time of the acceleration maximum, t_m, the peak value of the acceleration, a_m, and the average acceleration, $\overline{a}$.

The method for deriving the velocity and acceleration time-profiles is based on the cubic-spline smoothing of the distance – time data in the interval covering the CME acceleration stage (for details see Maričić *et al.* (2004)). From two successive smoothed data points, we evaluated the instantaneous velocity:

$$v(t_{vi}) = \frac{r(t_{i+1}) - r(t_i)}{t_{i+1} - t_i}\,, \tag{1}$$

where $t_{vi} = (t_{i+1} + t_i)/2$. The acceleration is obtained from two successive velocity data points:

$$a(t_{ai}) = \frac{v(t_{vi+1}) - v(t_{vi})}{t_{vi+1} - t_{vi}}\,, \tag{2}$$

where $t_{ai} = (t_{vi+1} + t_{vi})/2$. The average acceleration is estimated applying:

$$\overline{a} = \frac{v_m - v_b}{t_{vm} - t_b}\,, \tag{3}$$

where v_m is the peak velocity, v_b is the velocity at the onset of the acceleration phase, whereas t_{vm} and t_b are the corresponding times, determined from the velocity time profile. Note that in an ideal situation t_{vm} and t_e should be identical, but in real situations they usually have different values, since $a(t)$ often shows several "oscillations" around $a = 0$ at the end of the acceleration stage. In most of the 18 analyzed events, the acceleration phase duration is estimated with a similar accuracy, generally ranging between 10 – 20%.

In Table 1 we present the list of the 18 analyzed events, ordered by the observation date. In the first three columns we present the event label, the date, and the first-appearance time of CMEs in the LASCO-C2 (hereafter, we use the event labels instead of dates, *e.g.*, the first event on the list will be denoted simply as E1, the second as E2, *etc.*). The highest speeds v_m of LEs and EPs, determined from the $v(t)$ profiles, are displayed in columns 4 and 5 of Table 1. Columns 6 and 7 show peak accelerations a_m of LEs and EPs determined from the $a(t)$ profiles, whereas in columns 8 and 9 we present the mean accelerations $\overline{a}$ of LEs and EPs.

The temporal characteristics of the acceleration phase are given in Table 2, where the first column represents the event label. In columns 2 and 3 the acceleration phase durations ($T_a = t_e - t_b$) of LE and EP are listed. From the obtained timing information, we estimated the time differences between the beginnings, the peaks, and the ends of the acceleration phases of LEs and EPs (denoted as Δt_b, Δt_m, and Δt_e, respectively). These time differences are presented in columns 4 – 6. Since the time differences, as well as the related errors, obviously depend

Table 1 Kinematical properties of the analyzed events.

Label	Date	LASCO [UT]	v_{mLE} [km s^{-1}]	v_{mEP} [km s^{-1}]	a_{mLE} [m s^{-2}]	a_{mEP} [m s^{-2}]	$\bar{a}_{LE}$ [m s^{-2}]	$\bar{a}_{EP}$ [m s^{-2}]
E1	26 02 2000	23:54	778	469	234	164	146	88
E2	28 06 2000	19:31	1466	626	1293	403	484	243
E3	23 04 2001	19:09	365	273	40	17	20	8
E4	25 05 2001	17:26	958	961	300	299	170	168
E5	08 01 2002	18:30	480	275	120	93	57	48
E6	09 03 2002	22:30	371	290	270	150	128	41
E7	06 06 2002	17:54	745	534	90	70	54	42
E8	16 02 2003	23:08	491	461	270	69	107	47
E9	18 02 2003	02:42	802	693	209	182	87	74
E10	14 03 2003	18:06	881	642	382	330	151	103
E11	15 03 2003	21:54	629	475	76	62	38	27
E12	26 04 2003	21:50	705	427	193	154	89	71
E13	15 07 2003	22:30	540	568	132	268	46	137
E14	21 10 2003	19:54	640	471	51	73	29	31
E15	12 11 2003	18:30	940	670	363	164	241	99
E16	18 08 2004	17:54	740	534	766	160	389	95
E17	06 09 2005 I	20:00	1235	998	244	246	162	133
E18	06 09 2005 II	21:12	715	665	40	39	171	14
Average			749	557	281	136	134	81
Std.dev.			282	202	305	108	126	59

on the duration of the event itself, we also employ the normalized time differences, where we divide a given lag by the duration of the LE acceleration phase. These normalized lags, $\Delta t_b/T_a$, $\Delta t_m/T_a$, and $\Delta t_e/T_a$, are presented in columns 7 – 9 of Table 2. In the last two rows of Tables 1 and 2, the average values and standard deviations are given. The average value of LE peak velocities is 749 km s^{-1}, while the average peak acceleration equals to 281 m s^{-2}. The corresponding values for EPs are 557 km s^{-1} and 136 m s^{-2}, respectively.

3. Results

In Figures 1a and c we show the distribution of peak velocities of LEs and EPs. The histograms show that the LE distribution has maximum at the bin 600 – 800 km s^{-1}, and for the EP the peak is at the bin 400 – 600 km s^{-1}.

Distributions of LE and EP peak accelerations are shown in Figures 1b and d, respectively. Peak accelerations of LEs vary from 40 up to 1300 m s^{-2}, while for EPs they vary from 17 up to 500 m s^{-2}. The peak accelerations are roughly twice as large as the mean accelerations (compare columns 6 and 7 with columns 8 and 9 of Table 1). The distributions show that velocities and accelerations are significantly larger for LEs then for EPs.

Distributions of the LE and the EP acceleration phase durations are shown in Figures 2a and b. The acceleration phase duration for LEs ranges from 35 min up to 10 h, and similarly, for EPs it varies from 50 min up to 10 h. The distribution peaks, for both LE and EP, at the

Table 2 The timing characteristics of the acceleration phase.

Event	T_{aLE} [min]	T_{aEP} [min]	Δt_b [min]	Δt_m [min]	Δt_e [min]	$\Delta t_b/T_a$	$\Delta t_m/T_a$	$\Delta t_e/T_a$
E1	113	113	18.3	−6.7	18.3	0.16	−0.06	0.16
E2	57	50	9.6	−8.3	16.7	0.17	−0.15	0.29
E3	330	388	41.7	3.3	−16.7	0.13	0.01	−0.05
E4	122	105	−1.3	−4.7	15.9	−0.01	−0.04	0.13
E5	161	112	3.2	−5.6	52.5	0.02	−0.04	0.33
E6	48	115	3.3	−33.3	−63.3	0.07	−0.69	−1.31
E7	240	215	−8.3	18.3	16.7	−0.04	0.08	0.07
E8	85	152	5.0	−15.0	−61.7	0.06	−0.18	−0.73
E9	151	151	0.0	0.5	0.0	0.00	0.00	0.00
E10	57	103	43.3	−36.7	−3.3	0.77	−0.65	−0.06
E11	295	213	−3.3	−15.0	78.3	−0.01	−0.05	0.27
E12	153	120	−10.0	−16.7	23.3	−0.07	−0.11	0.15
E13	105	67	−63.3	−31.7	−25.0	−0.60	−0.30	−0.24
E14	460	285	−51.7	−1.7	123.3	−0.11	0.00	0.27
E15	63	92	1.7	−1.7	−26.7	0.03	−0.03	−0.42
E16	35	90	35.0	−11.7	−20.0	1.00	−0.33	−0.57
E17	165	155	−3.3	3.3	6.7	−0.02	0.02	0.04
E18	593	593	−1.7	3.3	116.7	0.00	0.01	0.20
Average	179	173	1.0	−8.9	14.0	0.09	−0.14	−0.08
Std.dev.	152	133	26.8	14.2	51.9	0.33	0.22	0.43

bin 100 – 200 min (the mean value for the LE is 179 min, while for the EP is 173 min). Thus, distributions of the acceleration phase duration are practically equal.

Inspecting columns 5 and 8 of Table 2 one finds that the acceleration peak of LE is closely associated with the acceleration peak of EP in the majority of events. The distribution of delays Δt_m, presented in Figure 3, peaks at $\Delta t_m = 0$, yet showing an asymmetry towards $\Delta t_m < 0$. The mean delay is $\Delta t_m = -9 \pm 14$ min (negative value means that the acceleration peak of LE occurs before the acceleration peak of EP). Bearing in mind the accuracy of measurements and data reduction procedure, we consider such a behavior as a very close synchronization. However, we emphasize that the time difference in several events is larger than 30 min.

The scatter of time-lags becomes somewhat larger if the time differences between the onsets or ends of the acceleration phases are considered. This is not surprising, since determining the onset and end times is more ambiguous than the estimate of peak times (for details see Maričić *et al.* (2004)). Distributions of these time lags have mean values $\Delta t_b = 1 \pm 26$ min and $\Delta t_e = 14 \pm 52$ min, respectively.

As already mentioned, to eliminate the effect of different time scales involved (events of longer duration show larger time differences), we normalized the delays by dividing them by the duration of the LE acceleration phase. In columns 7 – 9 of Table 2 these normalized time differences, $\Delta t_b/T_a$, $\Delta t_m/T_a$, and $\Delta t_e/T_a$, are presented. Inspecting column 8 of Table 2, we find that normalized time differences between the peak acceleration of LE and EP, $\Delta t_m/T_a$, range from -0.69 to $+0.08$. The distribution of $\Delta t_b/T_a$, $\Delta t_m/T_a$, and $\Delta t_e/T_a$ are shown in Figures 4a – c, respectively. Distributions are characterized by mean values $\Delta t_b/T_a =$

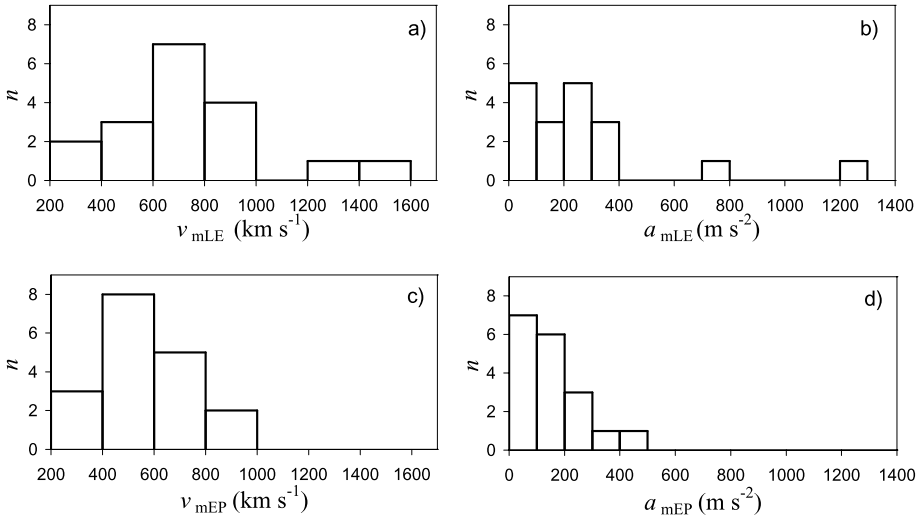

Figure 1 Distribution of: (a) LE peak velocities; (b) LE peak accelerations; (c) EP peak velocities; (d) EP peak accelerations.

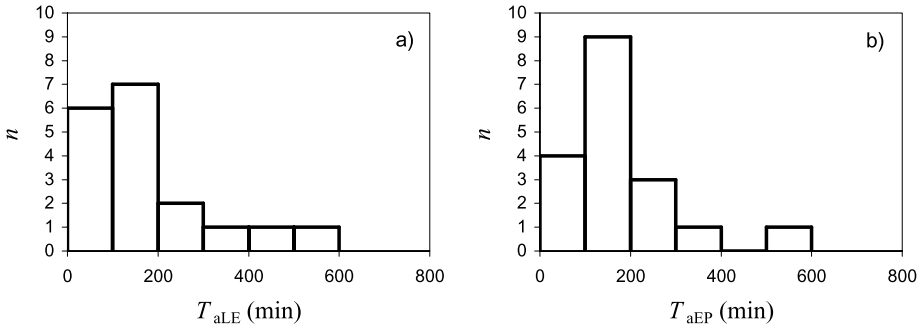

Figure 2 Distribution of acceleration phase durations for: (a) LEs (the shortest observed acceleration phase duration was 35 min); (b) EPs (the shortest observed acceleration phase duration was 50 min).

0.09 ± 0.32, $\Delta t_m / T_a = -0.14 \pm 0.22$, and $\Delta t_e / T_a = -0.08 \pm 0.43$. This clearly shows that in most events LE and EP acceleration phases are well synchronized, with lags ranging on average around $\pm 10\%$. More specifically, in 14 out of 18 events (78%) the beginning of the acceleration phase of LE and EP is synchronized to within ± 20 min. However, in events E3 and E10 the EP starts to accelerate 40 min earlier than the LE, whereas in events E13 and E14 the LE starts to accelerate more than 50 min earlier than the EP. So, in these four events there was a considerable mismatch between the beginning of the acceleration phases of LE and EP.

In Figure 5 we show the relationship between peak speeds of LEs and EPs. The graph shows a linear dependence, *i.e.*, larger speeds of LEs on average are associated with larger speeds of EPs. All data points are located above the $y = x$ line, *i.e.*, the highest speed of LE is always larger than the highest speed of EP. In Figure 5 we also present a fit of the form $y = kx$. The linear dependence is characterized by the slope $k = 1.31$, the correlation coefficient $C = 0.71$, and the F-test of statistical significance $P > 99\%$. Note that the event

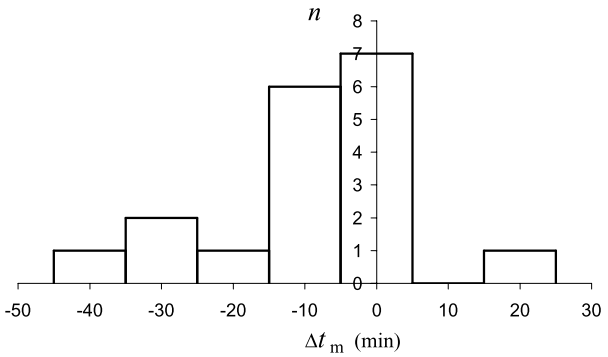

Figure 3 Distribution of the time lags between the acceleration peaks of LEs and EPs. Negative values mean that the acceleration peak of LE occurs before the acceleration peak of EP.

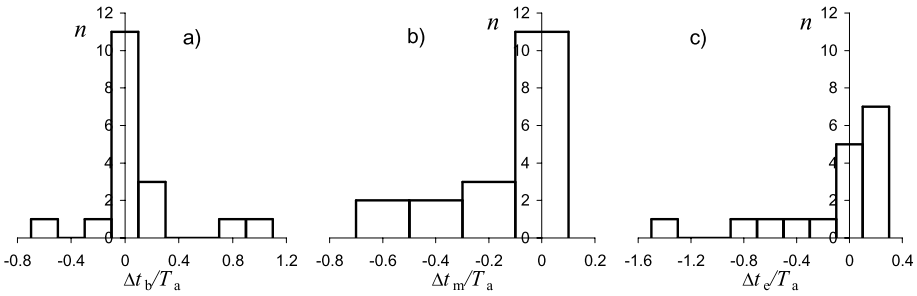

Figure 4 Distribution of normalized time differences between: (a) the beginning of the acceleration phase of LE and EP; (b) the acceleration peak of LE and EP; and (c) the end of acceleration phase of LE and EP. Note a different scale of the x-axis in the middle graph.

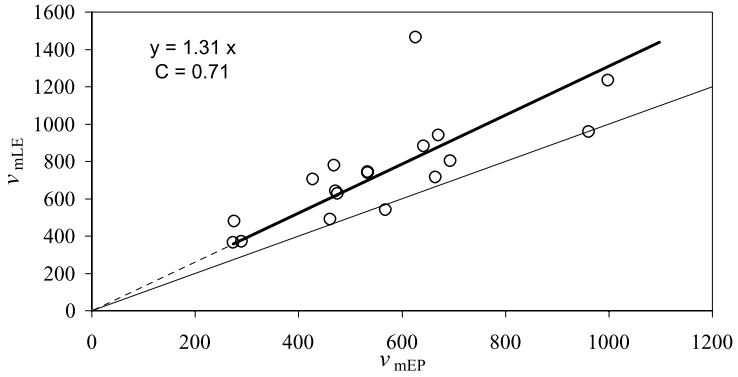

Figure 5 LE peak velocities shown as a function of the EP peak velocities. The linear least squares fit of the form $y = kx$ is drawn by bold line; the fit parameters are given in the inset together with the correlation coefficient C. Thin line represents the $y = x$ line. Errors of individual values of the velocity are smaller then the scatter of data-points.

E2, having the highest v_{mLE}, seems to be an extreme not belonging to the rest of the sample. If it were to be removed, the correlation coefficient would increase to $C = 0.84$ and the slope would decrease to $k = 1.24$.

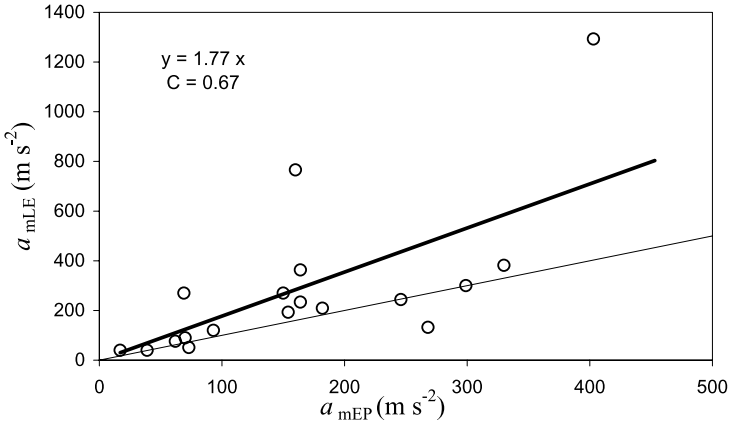

Figure 6 LE peak-accelerations shown as a function of EP peak-accelerations. The linear least squares fit of the form $y = kx$ is shown by bold line; the fit parameters are given in the inset together with the correlation coefficient C. Thin line represents the $y = x$ line. Errors of individual values of the acceleration are smaller then the scatter of data-points.

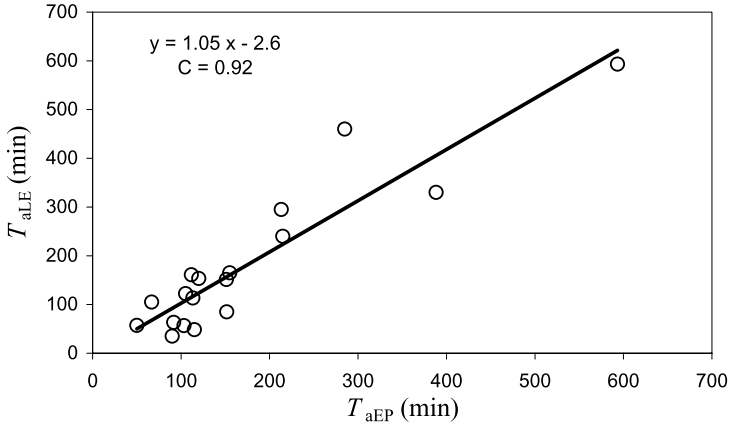

Figure 7 Relationship between the duration of LE and EP acceleration phases. The F-test statistical significance of the correlation is $P > 99\%$.

The correlation of peak accelerations of LEs and EPs is shown in Figure 6. The graph reveals that LE accelerations are almost two times larger than EP accelerations ($a_{mLE} = 1.77\, a_{mEP}$, with $C = 0.67$). If the data were fitted by the power-law, one would get $a_{mLE} = 2.14\, a_{mEP}^{0.92}$, with even higher correlation coefficient, $C = 0.79$. Similar results are obtained for mean accelerations: $\overline{a}_{LE} = 1.63\, \overline{a}_{EP}$ with $C = 0.67$ and $\overline{a}_{LE} = 2.39\, \overline{a}_{EP}^{0.89}$ with $C = 0.82$, respectively.

In Figure 7 we present the correlation between the acceleration phase durations of LEs and EPs. On average, longer acceleration phase of LE is associated with longer acceleration phase of EP. The graph shows a linear dependence between these two parameters, characterized by the slope $k = 1.05$, the correlation coefficient $C = 0.92$, and F-test statistical significance larger than 99%. This reveals that acceleration phase duration is practically equal for LEs and EPs.

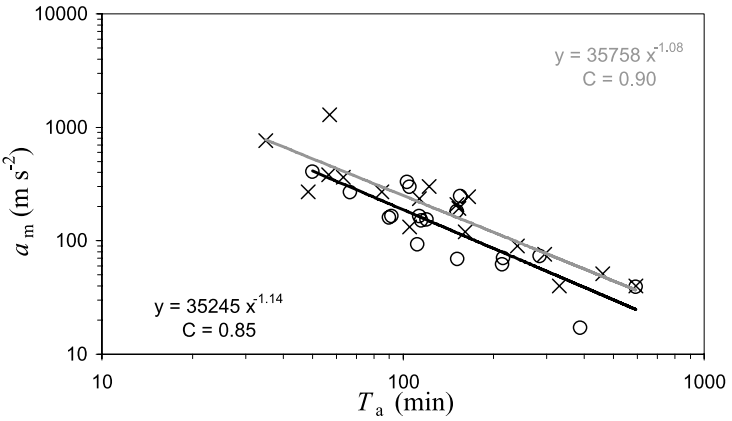

Figure 8 LE peak acceleration shown as a function of the LE acceleration phase duration (crosses and gray line). The same is shown for EPs by black circles. The F-test statistical significance of both correlations is $P > 99\%$.

Inspecting columns 6 and 7 of Table 1, and comparing them with columns 2 and 3 of Table 2, one finds that weaker accelerations of LEs and EPs are associated with longer acceleration phase duration. In Figure 8 we show this anticorrelation, characterized by the power-law dependence $a_{\rm LE} = 3.6 \times 10^4\ T_{\rm aLE}^{-1.08}$ and $a_{\rm EP} = 3.5 \times 10^4\ T_{\rm aEP}^{-1.14}$, respectively, where $T_{\rm a}$ is expressed in minutes and $a_{\rm m}$ in m s^{-2}. Such a relationship is very similar to that found for LEs by Vršnak *et al.* (2007). Let us also note that Zhang (2005), Zhang and Dere (2006), and Vršnak *et al.* (2007) found an analogous anticorrelation for average accelerations of LEs (the power-law slope ≈ -1). Note that the $a_{\rm m}(T_{\rm a})$ relationship shown in Figure 8 is practically the same for LEs and EPs.

4. Summary and Discussion

Our results are summarized as follows:

1. Peak speeds of LEs are on average around 30% higher than peak speeds of EPs (Figure 5, Table 1).
2. Peak accelerations of LEs are almost two times larger than the EP peak accelerations (Figure 6, Table 1).
3. The acceleration phase durations of LEs are on average equal to that of EPs, (Figure 7, Table 2).
4. In the majority of events (78%) the acceleration of LE and EP begins almost simultaneously (within ± 20 min), however, in two events the EP acceleration began considerably earlier than the LE acceleration (> 40 min) and in two events the LE acceleration started > 50 min before the EP acceleration.
5. Peak accelerations of LEs and EPs are closely synchronized in most events (the distribution has maximum at $\Delta t = 0$); however, time differences in some events are larger than 30 min (Table 2) and there is a tendency that, in a fraction of events, the LE acceleration peaks earlier than in EP (Figure 4b).
6. In most of the events the beginning and the end of the acceleration phase of EP and LE are synchronized, with a tendency that, in some events, EP starts to accelerate earlier and ends accelerating after the LE (Figures 4a and c, respectively).

7. Durations of the acceleration phase are anticorrelated with the corresponding peak accelerations for LEs, as well as for EPs (Figure 8).

Our results show that acceleration phases of LEs and EPs are closely correlated in the majority of events, confirming the suggestion by Gopalswamy *et al.* (2003) that the prominence eruption starts simultaneously with the CME take-off. Moreover, the presented results, for the first time, quantitatively demonstrate that the acceleration phase most often develops in a "self-similar" manner, like in the event described by Maričić *et al.* (2004).

This means that LE and EP, in the majority of cases, behave as parts of a common erupting magnetic structure. Such behavior favors the flux-rope CME models (*e.g.*, Chen, 1989; Vršnak, 1990; Amari *et al.*, 2003; Török and Kliem, 2005; Lin, 2004; Gibson *et al.*, 2006; *etc.*) where the prominence is nested in "magnetic dips" below the rope axis (Demoulin and Priest, 1989), whereas the upper parts of the rope represent the leading edge. In this type of model, the flux-rope loses equilibrium (*e.g.*, due to the poloidal flux injection, *i.e.*, the increase of the axial current) as one entity, so the eruption proceeds in a self-similar manner. However, it should be noted that flux-rope models only occasionally take into account quantitatively the variation of the density within the rope (dense/inert prominence plasma below the rope axis, lighter parts above the axis). For example, such a situation was considered in the numerical simulation by Gibson and Fan (2006), but they did not present the kinematics of the eruption quantitatively, thus no direct comparisons with the observed kinematics are possible.

On the other hand, in the models based on the so-called tether-cutting mechanism (Moore and Roumeliotis, 1992; Moore *et al.*, 2001) the synchronization of the LE and EP acceleration should happen only occasionally: The eruption is expected to start by the upward motion of those structural elements that are affected by reconnection between the existing magnetic structure and, *e.g.*, the newly emerging flux. This could either be the external part of the structure (becoming the leading edge of the eruption), or its core (presumably imbedding the prominence), depending on where the new flux emerges. Thus, the tether-cutting type of process might be attributed to those events where the acceleration of LE and EP are not synchronized.

A similar conclusion could be drawn regarding the models based on the break-out mechanism (Antiochos, 1998), where the CME take-off is a consequence of the reconnection between the rising structure and the overlaying field. Thus, two (or more) separate magnetic structures take part in the eruption, as proposed by Srivastava *et al.* (2000), to explain the different behavior of LE and EP in the event they studied. In particular a "standard" version of the break-out model could explain the delay of LE formation/acceleration (see, *e.g.*, MacNeice *et al.*, 2004), whereas its modification proposed by Van der Holst, Jacobs, and Poedts (2007) could explain the opposite situation (see Figure 3 therein).

Given the above discussion, our results favor the flux-rope loss-of-equilibrium process as the most likely mechanism for the CME take-off in the majority of eruptions. Further strong arguments are the close synchronization of the acceleration phase and the energy release in the associated flare (*e.g.*, Maričić *et al.*, 2007; for the physical background see Lin (2004) and Vršnak (2008)), and the fact that the acceleration usually peaks when the height of the erupting structure becomes comparable with the footpoint half-separation (Vršnak, Ruždjak, and Rompolt, 1991; for the explanation see Chen and Krall (2003)). However, our results also show that in some cases other mechanisms, such as those described by tether-cutting or break-out models, could be driving the eruption.

Acknowledgements We are grateful to the MLSO and SoHO teams for developing and operating the instruments and we appreciate their open data policies. We are thankful to the referee, whose comments

helped us to put our results in a wider context. The research leading to the results presented in this article received funding from European Community's Seventh Framework Programme (FP7/2007-2013) under grant agreement no. 218816.

References

Amari, T., Luciani, J.F., Aly, J.J., Mikic, Z., Linker, J.: 2003, *Astrophys. J.* **585**, 1073.
Andrews, M.D., Howard, R.A.: 2001, *Space Sci. Rev.* **95**, 147.
Antiochos, S.K.: 1998, *Astrophys. J.* **502**, L181.
Brueckner, G.E., Howard, R.A., Koomen, M.J., Korendyke, C.M., Michels, D.J., Moses, J.D., *et al.*: 1995, *Solar Phys.* **162**, 357.
Chen, J.: 1989, *Astrophys. J.* **338**, 453.
Chen, J., Krall, J.: 2003, *J. Geophys. Res.* **108**, 1410.
Delaboudiniere, J.P., Artzner, G.E., Brunaud, J., Gabriel, A.H., Hochedez, J.F., Millier, F., *et al.*: 1995, *Solar Phys.* **162**, 291.
Demoulin, P., Priest, E.R.: 1989, *Hvar Obs. Bull.* **13**, 261.
Dere, K.P., Brueckner, G.E., Howard, R.A., Michels, D.J., Delaboudiniere, J.P.: 1999, *Astrophys. J.* **516**, 465.
Engvold, O.: 1987. In: Priest, E.R. (ed.) *Dynamics and Structure of Solar Prominences*, Kluwer Academic, Dordrecht, 47.
Filippov, B.: 1998, In: Webb, D.F., Schmieder, B., Rust, D.M. (eds.) *New Perspectives on Solar Prominences, IAU Colloq.* **167**, 342.
Filippov, B., Koutchmy, S.: 2008, *Ann. Geophys.* **26**, 3025.
Fisher, R., Garcia, C.J., Seagraves, P.: 1981, *Astrophys. J.* **246**, L161.
Gallagher, P.T., Lawrence, G.R., Dennis, B.R.: 2003, *Astrophys. J.* **588**, L53.
Gibson, S.E., Fan, Y.: 2006, *J. Geophys. Res.* **111**, 12103.
Gibson, S.E., Fan, Y., Török, T., Kliem, B.: 2006, *Space Sci. Rev.* **124**, 131.
Gopalswamy, N.: 2006, *Space Sci. Rev.* **124**, 145.
Gopalswamy, N., Shimojo, M., Lu, W., Yashiro, S., Shibasaki, K., Howard, R.A.: 2003, *Astrophys. J.* **586**, 562.
House, L.L., Wagner, W.J., Hildner, E., Sawyer, C., Schmidt, H.U.: 1981, *Astrophys. J.* **244**, L117.
Hundhausen, A.: 1987, In: Pizzo, V.J., Holzer, T., Sime, D.G. (eds.) *Sixth International Solar Wind Conference*, 181.
Hundhausen, A.: 1999, In: Strong, K.T., Saba, J.L.R., Haisch, B.M., Schmelz, J.T. (eds.) *The Many Faces of the Sun: A Summary of the Results from NASA's Solar Maximum Mission*, 143.
Illing, R.M.E., Hundhausen, A.J.: 1985, *J. Geophys. Res.* **90**, 275.
Koutchmy, S., Slemzin, V., Filippov, B., Noens, J.C., Romeuf, D., Golub, L.: 2008, *Astron. Astrophys.* **483**, 599.
Krall, J., Chen, J., Duffin, R.T., Howard, R.A., Thompson, B.J.: 2001, *Astrophys. J.* **562**, 1045.
Lin, J.: 2004, *Solar Phys.* **219**, 169.
Low, B.C., Hundhausen, A.J.: 1987, *J. Geophys. Res.* **92**, 2221.
MacNeice, P., Antiochos, S.K., Phillips, A., Spicer, D.S., DeVore, C.R., Olson, K.: 2004, *Astrophys. J.* **614**, 1028.
Maričić, D., Vršnak, B., Stanger, A.L., Veronig, A.: 2004, *Solar Phys.* **225**, 337.
Maričić, D., Vršnak, B., Stanger, A.L., Veronig, A.M., Temmer, M., Roša, D.: 2007, *Solar Phys.* **241**, 99.
Moore, R.L., Roumeliotis, G.: 1992, In: Svestka, Z., Jackson, B.V., Machado, M.E. (eds.) *Eruptive Solar Flares, IAU Colloq.* **133**, 69.
Moore, R.L., Sterling, A.C., Hudson, H.S., Lemen, J.R.: 2001, *Astrophys. J.* **552**, 833.
Munro, R.H., Gosling, J.T., Hildner, E., MacQueen, R.M., Poland, A.I., Ross, C.L.: 1979, *Solar Phys.* **61**, 201.
Plunkett, S.P., Brueckner, G.E., Dere, K.P., Howard, R.A., Koomen, M.J., Korendyke, C.M., *et al.*: 1997, *Solar Phys.* **175**, 699.
Plunkett, S.P., Vourlidas, A., Šimberová, S., Karlický, M., Kotrč, P., Heinzel, P., *et al.*: 2000, *Solar Phys.* **194**, 371.
Schmahl, E., Hildner, E.: 1977, *Solar Phys.* **55**, 473.
Srivastava, N., Schwenn, R., Inhester, B., Martin, S.F., Hanaoka, Y.: 2000, *Astrophys. J.* **534**, 468.
Török, T., Kliem, B.: 2005, *Astrophys. J.* **630**, L97.
van der Holst, B., Jacobs, C., Poedts, S.: 2007, *Astrophys. J.* **671**, L77.
Vršnak, B.: 1990, *Solar Phys.* **129**, 295.
Vršnak, B.: 2001, *J. Geophys. Res.* **106**, 25249.

Vršnak, B.: 2008, *Ann. Geophys.* **26**, 3089.
Vršnak, B., Ruzdjak, V., Rompolt, B.: 1991, *Solar Phys.* **136**, 151.
Vršnak, B., Sudar, D., Ruždjak, D.: 2005, *Astron. Astrophys.* **435**, 1149.
Vršnak, B., Maričić, D., Stanger, A.L., Veronig, A.M., Temmer, M., Roša, D.: 2007, *Solar Phys.* **241**, 85.
Webb, D.F., Hundhausen, A.J.: 1987, *Solar Phys.* **108**, 383.
Webb, D.F., Krieger, A.S., Rust, D.M.: 1976, *Solar Phys.* **48**, 159.
Williams, D.R., Török, T., Démoulin, P., van Driel-Gesztelyi, L., Kliem, B.: 2005, *Astrophys. J.* **628**, L163.
Wood, B.E., Karovska, M., Chen, J., Brueckner, G.E., Cook, J.W., Howard, R.A.: 1999, *Astrophys. J.* **512**, 484.
Zhang, J.: 2005, In: Dere, K., Wang, J., Yan, Y. (eds.) *Coronal and Stellar Mass Ejections, IAU Symp.* **226**, 65.
Zhang, J., Dere, K.P.: 2006, *Astrophys. J.* **649**, 1100.
Zhang, J., Dere, K.P., Howard, R.A., Kundu, M.R., White, S.M.: 2001, *Astrophys. J.* **559**, 452.
Zhang, J., Dere, K.P., Howard, R.A., Vourlidas, A.: 2004, *Astrophys. J.* **604**, 420.